Inorganic Chemistry

Article

pubs.acs.org/IC

Facile Growth of Thermochromic VO_2 Nanostructures with Greatly Varied Phases and Morphologies

Ying-Ting Wang and Chun-Hua Chen*

Department of Materials Science and Engineering, National Chiao Tung University, 1001 Ta-Hsueh Road, Hsin-Chu, Taiwan, 30010, Republic of China

ABSTRACT: We have successfully and reproducibly synthesized a variety of novel vanadium dioxide (VO_2) nanostructures, including metastable monoclinic VO_2(B) nanoneedles and nanocorals, orthorhombic VO_2(O) nanoparticles, and monoclinic VO_2(M) nanofacets by manipulating the aging time of a facile sol−gel approach and the subsequent postannealing conditions. We envision that this previously unreported highly controlled synthesis and the resulting distinct morphologies of VO_2 will not only provide a promising route for reliably selecting the phase, size, and morphology of these nanostructures, as well as achieving a fundamental understanding of their unusual temperature-dependent optical transmittance, but also facilitate the synthesis of functional VO_2 nanostructures for a number of novel applications.

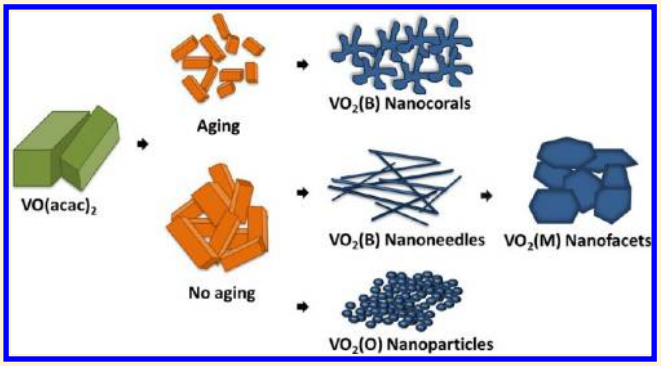

INTRODUCTION

Vanadium dioxide (VO_2), the most well-known of many vanadium-related oxides, has received considerable attention in recent years due to its interesting temperature-dependent optical and electrical properties induced by reversible phase transformation between monoclinic VO_2(M) and tetragonal VO_2(R) forms near room temperature. VO_2 has been used in a variety of applications, such as field-effect transistors,[1] electrical-optical switching devices,[2,3] memory,[4] switches,[5] smart windows,[6−8] flat panel displays,[9] and lithium batteries.[10]

In order to control the phase-transformation temperature and discover novel characteristics differing from their bulk counterparts,[2,11] considerable research effort has concentrated on synthesizing VO_2 nanostructures with specific morphologies, sizes, crystal structures, and dopants using various technologies including vapor transport,[1,3] sol−gel,[12,13] hydrothermal synthesis,[10] chemical vapor deposition,[7] pulsed laser ablation[14] and so on.[15−18] Among these studies, sol−gel methods, controlled simply by the concentration of the vanadium precursor, solvent, and surfactant and the reaction temperature, seem to be promising for larger-scale, faster, and lower-temperature syntheses of VO_2 nanostructures. However, as with other approaches, most of the prepared VO_2 nanostructures are one-dimensional (1-D) polycrystalline or single crystals, such as nanorods,[19] nanowires,[20] and nanorolls,[21] and a satisfactory level of systematic control is yet to be achieved over their size, dimension, uniformity, and stoichiometry.

In this work, we decided to synthesize VO_2 nanostructures by a relatively common, rapid, and reliable technique, i.e., the sol−gel method. By tuning the aging time of the precursors as well as the subsequent single or multiple heat treatments of the precursor-coated films, a series of VO_2 nanostructures with four unusual morphologies, namely, 0-D nanoparticles, 1-D nanoneedles, and distinct 3-D nanocorals and nanofacets belonging to three crystal systems (orthorhombic VO_2(O), monoclinic VO_2(M), and metastable monoclinic VO_2(B)), was successfully obtained for subsequent thermochromic characterization. To our knowledge, this is the first time a single facile approach has been used to systematically and reproducibly fabricate so many featured morphologies and crystal structures.

EXPERIMENTAL SECTION

Vanadium oxyacetylacetone ($VO(acac)_2$, 99.99%, Aldrich) was used as the only source of vanadium (V^{4+}) for synthesizing VO_2 nanocrystals. $VO(acac)_2$ (0.331 g) and methanol (95%, 1 mL) were ultrasonically mixed for 1 h at room temperature to form the precursor solution for film coating. To investigate the aging effect on the precursor and the resulting products, the well-mixed precursor solution was aged under an air atmosphere at room temperature for 24 h. After a long period of aging, the solution color changed from yellow-green to dark brown, indicating the partial reduction of V^{4+} ions. The fresh and aged precursor solutions (0.1 cm^3) were dropped onto ethanol-cleaned Si(100) substrates (1 × 1 cm^2) and underwent a drying process at 70 °C for 30 min to drive off the excess solvent. The dried specimens were first annealed in a N_2/H_2 (5 vol%) gas mixture (20 cm^3/min) at 550 °C for 30 min and then heated to 600 °C for 5 min to further increase the crystalline quality. In the case of VO_2(O), the same annealing processes were employed, but in a ~10^{-2} Torr atmosphere. The synthesized products were characterized with an X-ray diffractometer (XRD, Bruker D2), a field-emission scanning electron microscope (FE-SEM, JSM-6500), and a field-emission transmission electron microscope (FE-TEM, JEOL JEM-2100F). For FE-TEM observation, a trace amount of the prepared specimens was removed

Received: November 22, 2012
Published: February 18, 2013

   dx.doi.org/10.1021/ic302562j | Inorg. Chem. 2013, 52, 2550−2555

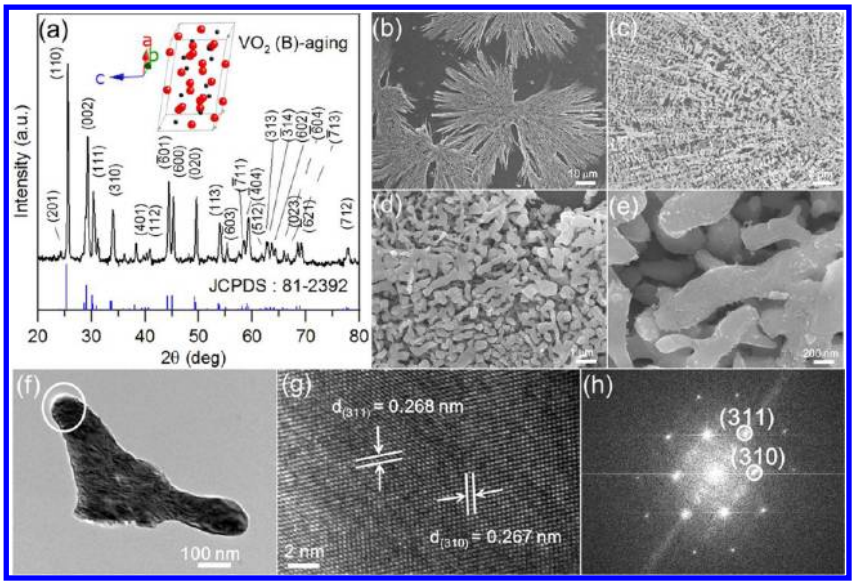

Figure 1. Metastable monoclinic VO_2(B) nanocorals synthesized from recipe #1: (a) XRD pattern, (b–e) SEM images, (f, g) HRTEM images, and (h) corresponding FFT pattern from (g).

from the substrates and then suspended in ethanol solution by ultrasonication. A drop of this suspension was placed onto a copper microgrid coated with an amorphous carbon film, followed with a drying process at 60 °C for 24 h in air. The temperature-dependent in situ transmission spectra were determined by a UV–vis–NIR spectrophotometer (JASCO V-630).

RESULTS AND DISCUSSION

Precursor Aging Effects on VO_2 Synthesis. In this work, excluding recipe #1, all the products were prepared from the fresh $VO(acac)_2$ methanol solution after 24 h of aging at room temperature. Figure 1a shows the XRD pattern of the product synthesized from recipe #1, as described in Table 1. The

Table 1. The Four Recipes Used to Synthesize VO_2 Nanostructures

	$VO(acac)_2$ Precursor	Heat Treatment	Products
1	24 h aging, RT	550 °C 30 min + 600 °C 5 min in H_2/N_2	Monoclinic VO_2(B) Nanocorals
2	No aging	550 °C 30 min + 600 °C 5 min in H_2/N_2	Monoclinic VO_2(B) Nanoneedles
3	No aging	550 °C 30 min + 600 °C 5 min in a vacuum	Orthorhombic VO_2(O) Nanoparticles
4	No aging	#2 + 600 °C 4 h second treatment in ambient atmosphere	Monoclinic VO_2(M) Nanofacets

specimens for XRD and subsequent SEM analyses were investigated in their received form, that is, without destructively removing them from the silicon substrate. As can be seen, all the reflections involving the Bragg angles and integrated intensities were indexed to VO_2(B) (JCPDS 81-2392), indicating randomly oriented polycrystallinity and high purity. The inset is the corresponding unit cell of monoclinic VO_2(B). The SEM images presented in Figure 1b–e obviously show a distinct coral-like morphology with an extremely high density of irregular branches, extending from a few origins up to several tens of micrometers away on the substrate. From the HRTEM image and the corresponding FFT (fast Fourier transformation) pattern of the head of one broken piece of a branch, as shown in Figure 1f–h, surprisingly, the whole branch is essentially a single crystal. Additionally, the very large and symmetrical butterfly-like shape, revealed in Figure 1b, could be the result of continuous and stable crystal growth; the nucleation sites are probably located at the symmetric center of each butterfly-like single crystal. On the basis of these results, it is reasonable to consider that the step of precursor aging plays an extremely critical role and provides the time required for the growth of such large crystals. Detailed investigations will be presented later.

Figure 2a shows the XRD pattern of the product prepared from recipe #2, which is essentially the same as recipe #1 except that the nonaged precursor was used. Basically, all the reflections could be indexed to VO_2(B) (JCPDS 81-2392), as shown in Figure 1a. However, the obvious variations in the relative peak intensities could have originated from the preferential orientation of the needle-like morphology, as can be seen in Figure 2b–f. The HRTEM image (Figure 2g) and the corresponding FFT pattern (Figure 2h) of the terminal of an isolated VO_2(B) nanoneedle evidently reveal single-crystalline growth along the [100] direction. In contrast to the irregular shapes obtained with recipe #1, such one-dimensional morphology is frequently reported for VO_2, especially for VO_2(B).[1,10,12,19] In addition to the isolated nanorods, higher-dimensional VO_2 nanostructures have also been synthesized, such as urchin-like nanoassemblies[22] or nanosheets.[23] In contrast to these interesting morphologies, in this work, we also discovered very unusual patterns assembled on the substrate by coral-like and needle-like VO_2(B), as shown in Figures 1b and 2b, respectively.

It is worth emphasizing that, via the facile preaging treatment, metastable monoclinic VO_2(B) nanocrystals with entirely dissimilar morphologies can be obtained with different growth patterns, i.e., continuous three-dimensional coral-like and isolated one-dimensional needle-like patterns. Obviously, the greatly varied morphology originates from the long aging

dx.doi.org/10.1021/ic302562j | Inorg. Chem. 2013, 52, 2550–2555

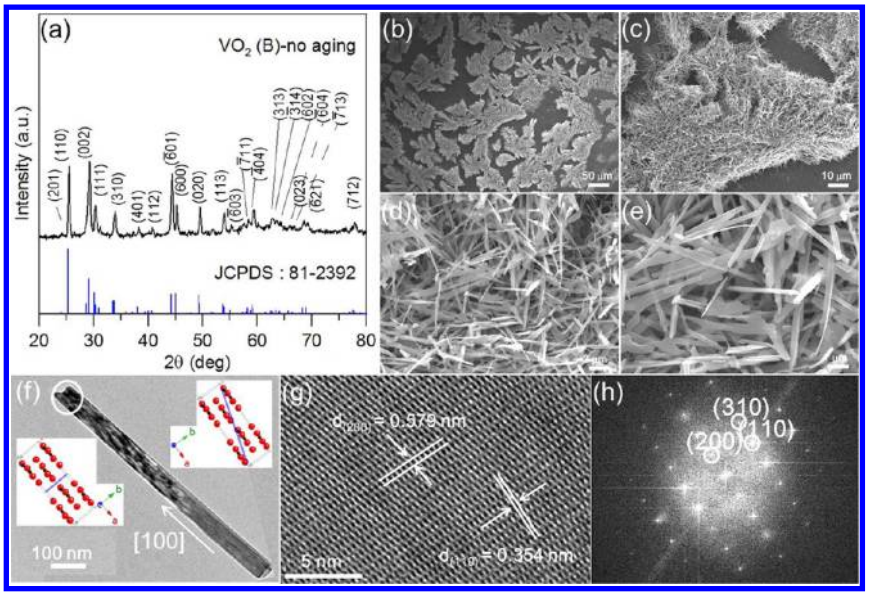

Figure 2. Metastable monoclinic VO_2(B) nanoneedles synthesized from recipe #2: (a) XRD pattern, (b–e) SEM images, (f, g) HRTEM images, and (h) corresponding FFT pattern from (g).

period of the $VO(acac)_2$. According to the XRD investigations on the nonaged and aged $VO(acac)_2$, as shown in Figure 3a and

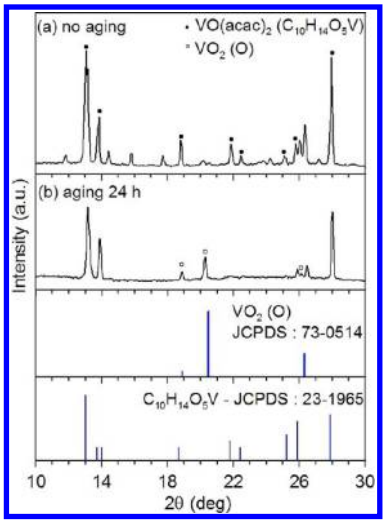

Figure 3. XRD patterns of the $VO(acac)_2$ precursor (a) before and (b) after 24 h of aging in aqueous methanol at room temperature.

b, respectively, slightly orthorhombic VO_2(O) (JCPDS 73-0514) spontaneously formed from the decomposition of $VO(acac)_2$ during the aging period in methanol solution at room temperature. The differences in the FTIR spectra around 3300–3500 cm^{-1}, as shown in Figure 4, also provide evidence of the presence of inorganic VO_2[24] in $VO(acac)_2$ after a long period of aging.

In the SEM image of the as-received $VO(acac)_2$ powders shown in Figure 5a, obvious rectangular crystal blocks can be found, suggesting that the present $VO(acac)_2$ probably prefers to form one-dimensional crystals and already exists in this form at the beginning due to the synthesis process. Thus, when $VO(acac)_2$ bundles are dispersed in methanol solution using ultrasonic treatment, they break into smaller blocks (Figure 5b, the case without aging) and begin to dissolve in the methanol. In the case of a long aging period, the SEM image (Figure 5c)

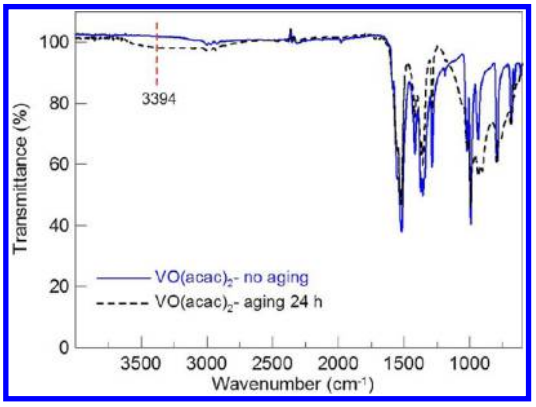

Figure 4. FTIR patterns of the $VO(acac)_2$ precursor before and after 24 h of aging in aqueous methanol at room temperature.

shows smaller irregular morphologies compared with Figure 5b. This suggests that the raw $VO(acac)_2$ powders are completely dissolved and new non-one-dimensional crystals of $VO(acac)_2$ and VO_2(O) are grown. It is reasonable to consider that the ultrasonic treatment and the long aging period, respectively, provide the energy and time needed to dissolve and recrystallize the $VO(acac)_2$. The presence of VO_2(O) crystals in the aging process probably results from direct decomposition of $VO(acac)_2$ with the required energy at the ultrasonic stage.

Although the role of pregrown VO_2(O) crystals is not clear at present, it is reasonable to consider that very small pieces of $VO(acac)_2$ blocks are formed after a long period of aging in methanol solution (see Figure 5a). The subsequent annealing treatment provides the energy required to decompose the $VO(acac)_2$ crystals and rearrange atoms to spontaneously form coral-like VO_2(B) single crystals along the substrate surface. In addition, we believe that needle-like VO_2(B) structures seen after high-temperature calcining are the products of an exfoliating process from larger pieces of $VO(acac)_2$ blocks, which also form in the same solution, but without aging (see Figure 5b), as has been previously observed.[25–27]

Since the final crystal structure and morphology of VO_2 are extremely sensitive to the annealing conditions, we also

dx.doi.org/10.1021/ic302562j | Inorg. Chem. 2013, 52, 2550–2555

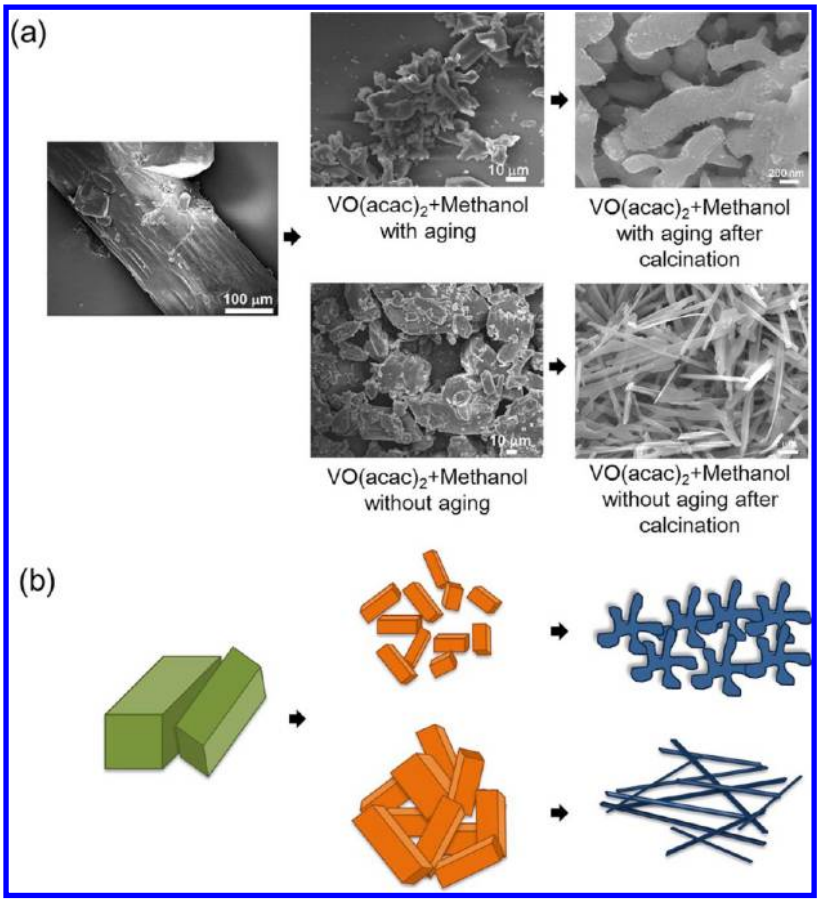

Figure 5. (a) SEM images of the as-received $VO(acac)_2$, the nonaged and aged $VO(acac)_2$ precursors, and the formed products. (b) The as-received bulk $VO(acac)_2$ disintegrated into much smaller pieces after a long period of aging.

annealed the aged $VO(acac)_2$ crystals from recipe #3 but under vacuum conditions (0.1 Torr) at a higher temperature (600 °C). Surprisingly, very tiny orthorhombic VO_2(O) nanoparticles (15 nm) were formed, as evidenced by the XRD pattern (JCPDS 73-0514) and the SEM image presented in Figure 6. To our knowledge, experimental data related to orthorhombic VO_2 are extremely lacking. Gui et al.[27] used a hydrothermal process, heating at 170 °C for 15 days to form needle-like orthorhombic VO_2 (~7 nm in width and ~35 nm in length). We believe the present aqueous solution-based method is a more facile way to synthesize very small orthorhombic VO_2 nanoparticles in a very high yield.

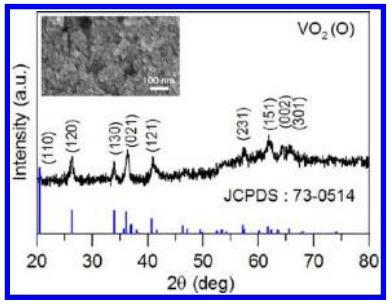

Figure 6. XRD pattern of the prepared orthorhombic VO_2(O) nanoparticles (recipe #3) and the corresponding SEM image (inset).

Secondary Annealing Effects on VO_2 Transformation. To demonstrate the effects of multiple annealings on the crystal structure and morphology of VO_2, the VO_2(B) nanoneedles were specially selected due to their noncontinuous microstructures for further secondary annealing processes. Figure 7a presents the XRD patterns of the products (#4) treated with a subsequent second annealing at 600 °C for 4 h under an ambient atmosphere. All reflections could be indexed by

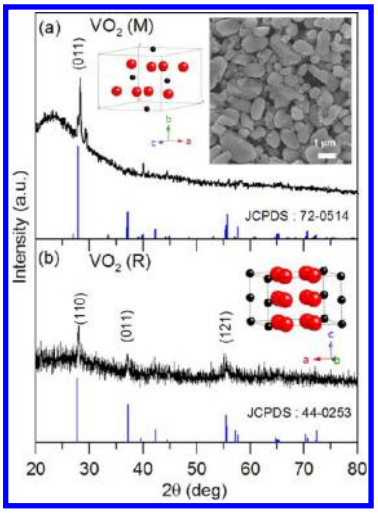

Figure 7. XRD patterns of the as-received monoclinic VO_2(M) (recipe #4) measured at (a) room temperature and (b) 90 °C. The unit cells of the monoclinic VO_2(M) and tetragonal VO_2(R) forms as well as the SEM image are also presented. Vanadium and oxygen atoms are shown as black and red balls, respectively.

dx.doi.org/10.1021/ic302562j | Inorg. Chem. 2013, 52, 2550−2555

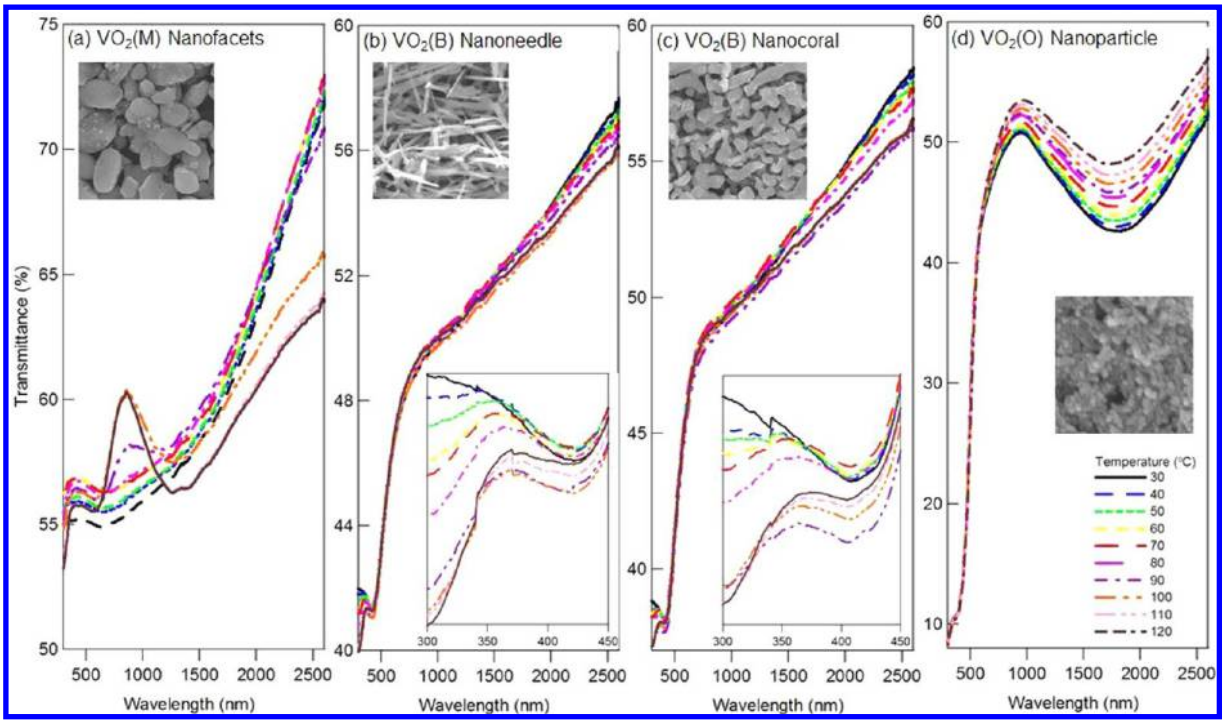

Figure 8. In situ UV−vis−NIR transmittance spectra of the prepared (a) VO_2(M) nanofacets, (b) VO_2(B) nanoneedles, (c) VO_2(B) nanocorals, and (d) VO_2(O) nanoparticles in a temperature range from 30 to 120 °C.

JCPDS 72-0514, indicating the formation of monoclinic VO_2(M). The SEM inset in Figure 7a displays coarse and irregular particles. A further increase in the annealing time up to 8 h did not change the monoclinic structure but led to slightly coarser particles. As is well-known, monoclinic VO_2(M) will convert to tetragonal VO_2(R) above a critical temperature, for instance, 68 °C for bulk materials,[28] and this phase transformation is generally reversible. Figure 7b shows the in situ XRD pattern measured at 90 °C under an N_2 atmosphere. As expected, the reflections can be indexed to VO_2(R) (JCPDS 44-0253).

Temperature-Dependent UV−Vis−NIR Transmittance Spectra. Figure 8 shows the temperature-dependent UV−vis−NIR transmittance spectra of the VO_2(M) nanofacets, VO_2(B) nanoneedles, VO_2(B) nanocorals, and VO_2(O) nanoparticles through a temperature range of 30 to 120 °C. As can be seen in Figure 8a, an abrupt variation in transmittance was initiated around 80−90 °C, which should be associated with the phase transformation from VO_2(M) to VO_2(R), as evidenced by the in situ XRD characterization (Figure 7). In addition to the weak temperature dependence of the transmittance peak at around 450 nm, another transmittance peak appeared at 850 nm in the temperature range 90−120 °C. Accompanying this peak, the transmittance of the NIR region (>1300 nm) simultaneously decreased. To clearly show the transmittance changes across the transition temperature, transmittances at specific wavelengths were selected for the plot of transmittance versus temperature, as shown in Figure 9a. Obviously, a drastic variation in transmittance occurred from ∼80 °C at all the selected wavelengths. This transmittance change became saturated when the temperature increased up to 110 °C. The transition starting and ending temperatures, as observed in Figure 9a, were much higher than those found in the bulk, polycrystalline,[29,30] and nanostructured VO_2 films.[31]

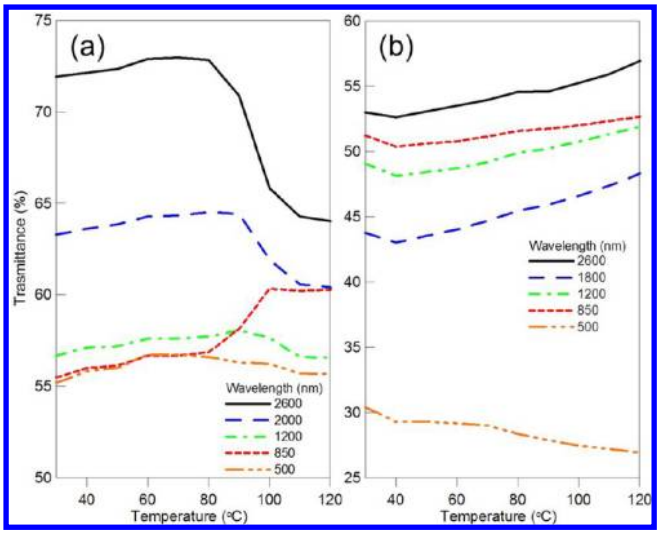

Figure 9. Temperature dependence of the UV−vis−NIR transmittance spectra of (a) VO_2(M) nanocrystals and (b) VO_2(O) nanoparticles at specific wavelengths from the visible to the NIR range.

The phenomenon of a size-dependent transition temperature has been widely observed in nanostructured VO_2. For instance, Lopez et al. synthesized a series of isolated VO_2 nanostructures (30−100 nm) by ion implantation into SiO_2 and found that a decrease in the equivalent size of VO_2 produced higher transition temperatures upon heating.[32] According to their data, nanoparticles larger than 80 nm exhibit a similar transition temperature to that of bulk VO_2 (68 °C). However, size should not be the only factor influencing the transition temperature; otherwise, the observed transition temperature of the present very large VO_2(M) nanofacets (∼1 μm) should be very close to 68 °C, instead of higher than 80 °C. Lopez et al. also suggested that the probability of triggering a structural phase transition at

dx.doi.org/10.1021/ic302562j | Inorg. Chem. 2013, 52, 2550−2555

a certain temperature decreases with decreasing nanoparticle size, as the number of defective sites for nucleation of the phase transformation within the relevant volume is reduced.[33] The much higher transition temperature observed in the present work might originate from the reduced presence of defective sites within VO_2(M) nanofacets for phase transformation. Similarly, increased transition temperatures (75−80 °C) were also found in the highly crystalline VO_2(M) nanorods with diameters of 50−100 nm and lengths of up to several micrometers.[34]

Figure 9b and c show the UV−vis−NIR transmittance spectra of the prepared VO_2(B) nanoneedles and nanocorals with uniform sizes, respectively. Less of a difference was observed between these two distinct VO_2(B) nanostructures, and the optical band gap estimated from the significant transmittance edges was ∼2.1 eV in both cases. Similar to the VO_2(B) nanostructures, the transmittance spectra of the VO_2(O) nanoparticles had no featured thermochromic properties, as shown in Figure 8d, but a much larger optical band gap of ∼2.5 eV was observed. Data related to the optical properties of VO_2(O) are extremely lacking. These special transmittance spectra obtained from various controlled morphologies and crystal structures are expected to provide new insight into the optics of assembled nanostructures.

■ CONCLUSION

A series of novel vanadium dioxide nanostructures, including metastable monoclinic VO_2(B) nanoneedles and nanocorals, orthorhombic VO_2(O) nanoparticles, and monoclinic VO_2(M) nanofacets, was successfully and reproducibly synthesized by manipulating the aging time of a facile sol−gel approach and the subsequent postannealing conditions. This is the first time that so many VO_2 phases with the featured morphologies could be obtained simultaneously using a single synthesis strategy. Additionally, we discovered that precursor aging evidently plays a very important and effective role in determining and creating the final distinct morphologies. The temperature-dependent UV−vis−NIR transmittance spectra of the nanostructured VO_2 films provided not only previously unobserved thermochromic data but new insights into the optics of nanocrystal assemblies.

■ AUTHOR INFORMATION

Corresponding Author

*E-mail: ChunHuaChen@mail.nctu.edu.tw. Tel: +886-3-5131287. Fax: +886-3-5724727.

Notes

The authors declare no competing financial interest.

■ REFERENCES

(1) Guiton, B. S.; Gu, Q.; Prieto, A. L.; Gudiksen, M. S.; Park, H. *J. Am. Chem. Soc.* **2005**, *127*, 498.
(2) Gentle, A.; Maaroof, A. I.; Smith, G. B. *Nanotechnology* **2007**, *18*, 025202.
(3) Sohn, J. I.; Joo, H. J.; Porter, A. E.; Choi, C. J.; Kim, K.; Kang, D. J.; Welland, M. E. *Nano Lett.* **2007**, *7*, 1570.
(4) Lee, M. J.; Park, Y.; Suh, D. S.; Lee, E. H.; Seo, S.; Kim, D. C.; Jung, R.; Kang, B. S.; Ahn, S. E.; Lee, C. B.; Seo, D. H.; Cha, Y. K.; Yoo, I. K.; Kim, J. S.; Park, B. H. *Adv. Mater.* **2007**, *19*, 3919−3923.
(5) Hu, B.; Zhang, Y.; Chen, W.; Xu, C.; Wang, Z. L. *Adv. Mater.* **2011**, *23*, 3536−3541.
(6) Manning, T. D.; Parkin, I. P.; Pemble, M. E.; Sheet, D.; Vernardou, D. *Chem. Mater.* **2004**, *16*, 744.
(7) Binions, R.; Hyett, G.; Piccirillo, C.; Parkin, I. P. *J. Mater. Chem.* **2007**, *17*, 4652.
(8) Balu, R.; Ashrit, P. V. *Appl. Phys. Lett.* **2008**, *92*, 021904.
(9) Gurvitch, M.; Luryi, S.; Polyakov, A.; Shabalov, A.; Dudley, M.; Wang, G.; Ge, S.; Yakovlev, V. *J. Appl. Phys.* **2007**, *102*, 033504.
(10) Armstrong, G.; Canales, J.; Armstrong, A. R.; Bruce, P. G. *J. Power Sources* **2008**, *178*, 723.
(11) Lopez, R.; Haglund, R. F.; Feldman, L. C.; Boatner, L. A.; Haynes, T. E. *Appl. Phys. Lett.* **2004**, *85*, 5191.
(12) Mai, L. Q.; Hu, B.; Hu, T.; Chen, W.; Gu, E. D. *J. Phys. Chem. B* **2006**, *110*, 19083.
(13) Baudrin, E.; Sudant, G.; Larcher, D.; Dunn, B.; Tarascon, J. M. *Chem. Mater.* **2006**, *18*, 4369.
(14) Lopez, R.; Haglund, R. F.; Feldman, L. C. *Appl. Phys. Lett.* **2006**, *88*, 081902.
(15) Balu, R.; Ashrit, P. V. *Appl. Phys. Lett.* **2008**, *92*, 021904.
(16) Lopez, R.; Boatner, L. A.; Haynes, T. E.; Feldman, L. C.; Haglund, R. F. *J. Appl. Phys.* **2002**, *92*, 4031.
(17) Peng, Z.; Jiang, W.; Liu, H. *J. Phys. Chem. C* **2007**, *111*, 1119.
(18) Li, X.; Chen, X.; Chen, X.; Han, C.; Shi, C. *J. Cryst. Growth* **2007**, *43*, 309.
(19) Corr, S. A.; Grossman, M.; Shi, Y.; Heier, K. R.; Stucky, G. D.; Seshadri, R. *J. Mater. Chem.* **2009**, *19*, 4362−4367.
(20) Baik, J. M.; Kim, M. H.; Larson, C. L.; Yavuz, C. T.; Stucky, G. D.; Wodtke, A. M.; Moskovits, M. *Nano Lett.* **2009**, *9*, 3980−3984.
(21) Sun, D.; Kwon, C. W.; Baure, G.; Richman, E.; MacLean, J.; Dunn, B.; Tolbert, S. H. *Adv. Funct. Mater.* **2004**, *14*, 12.
(22) Li, G.; Chao, K.; Zhang, C.; Zhang, Q.; Peng, H.; Chen, K. *Inorg. Chem.* **2009**, *48*, 3.
(23) Whittaker, L.; Zhang, H.; Banerjee, S. *J. Mater. Chem.* **2009**, *19*, 2968−2974.
(24) Channu, R.; Holze, R.; Rambabu, B.; Kalluru, R. R.; Williams, Q. L. *Int. J. Electrochem. Sci.* **2010**, *5*, 605−614.
(25) Leroux, Ch.; Nihoul, G.; Tendeloo, G. V. *Phys. Rev. B* **1998**, *57*, 5111−5121.
(26) Jiang, L.; Wei, M.; Ye, B.; Wei, K. *J. Cryst. Growth* **2008**, *310*, 4301−4304.
(27) Gui, Z.; Fan, R.; Chen, X. H.; Wu, Y. C. *J. Solid State Chem.* **2001**, *157*, 250−254.
(28) Chen, Z.; Gao, S.; Jiang, L.; Wei, M.; Wei, K. *Mater. Chem. Phys.* **2010**, *121*, 254−258.
(29) Nag, J.; Haglund, R. F. *J. Phys.: Condens. Matter* **2008**, *20*, 264016.
(30) Chen, S.; Ma, H.; Dai, J.; Yi, X. *Appl. Phys. Lett.* **2007**, *90*, 101117.
(31) Suh, J. Y.; Lopez, R.; Feldman, L. C.; Haglund, R. F. *J. Appl. Phys.* **2004**, *2*, 96.
(32) Lopez, R.; Haynes, T. E.; Boatner, L. A.; Feldman, L. C.; Haglund, R. F. *Phys. Rev. B* **2002**, *65*, 224113.
(33) Lopez, R.; Feldman, L. C.; Haglund, R. F. *Phys. Rev. Lett.* **2004**, *93*, 177403.
(34) Kam, K. C.; Cheetham, A. K. *Mater. Res. Bull.* **2006**, *41*, 1015−1021.